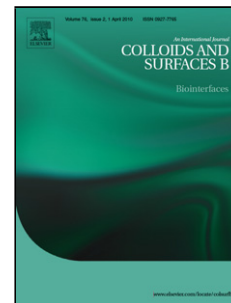


Accepted Manuscript

Title: Mesoporous Silica Nanoparticles Functionalized with Hyaluronic Acid. Effect of the Biopolymer Chain Length on Cell Internalization

Authors: Valentina Nairi, Silvia Magnolia, Marco Piludu, Mariella Nieddu, Cristian Antonio Caria, Valeria Sogos, Maria Vallet-Regi, Maura Monduzzi, Andrea Salis



PII: S0927-7765(18)30094-8
DOI: <https://doi.org/10.1016/j.colsurfb.2018.02.019>
Reference: COLSUB 9159

To appear in: *Colloids and Surfaces B: Biointerfaces*

Received date: 30-9-2017
Revised date: 3-2-2018
Accepted date: 10-2-2018

Please cite this article as: Valentina Nairi, Silvia Magnolia, Marco Piludu, Mariella Nieddu, Cristian Antonio Caria, Valeria Sogos, Maria Vallet-Regi, Maura Monduzzi, Andrea Salis, Mesoporous Silica Nanoparticles Functionalized with Hyaluronic Acid. Effect of the Biopolymer Chain Length on Cell Internalization, Colloids and Surfaces B: Biointerfaces <https://doi.org/10.1016/j.colsurfb.2018.02.019>

This is a PDF file of an unedited manuscript that has been accepted for publication. As a service to our customers we are providing this early version of the manuscript. The manuscript will undergo copyediting, typesetting, and review of the resulting proof before it is published in its final form. Please note that during the production process errors may be discovered which could affect the content, and all legal disclaimers that apply to the journal pertain.

Mesoporous Silica Nanoparticles Functionalized with Hyaluronic Acid. Effect of the Biopolymer Chain Length on Cell Internalization

Valentina Nairi¹, Silvia Magnolia¹, Marco Piludu², Mariella Nieddu², Cristian Antonio Caria³,
Valeria Sogos², Maria Vallet-Regi^{4,*}, Maura Monduzzi^{1,*}, and Andrea Salis^{1,*}

¹Dipartimento di Scienze Chimiche e Geologiche, Università di Cagliari-CSGI and CNBS, Cittadella Universitaria, S.S. 554 bivio Sestu, 09042 Monserrato (CA), Italy

²Dipartimento di Scienze Biomediche, Università di Cagliari, Cittadella Universitaria, S.S. 554 bivio Sestu, 09042 Monserrato (CA), Italy

³Istituto di Ricerca Genetica e Biomedica, Consiglio Nazionale delle Ricerche, Cittadella Universitaria, S.S. 554 bivio Sestu, 09042 Monserrato (CA), Italy

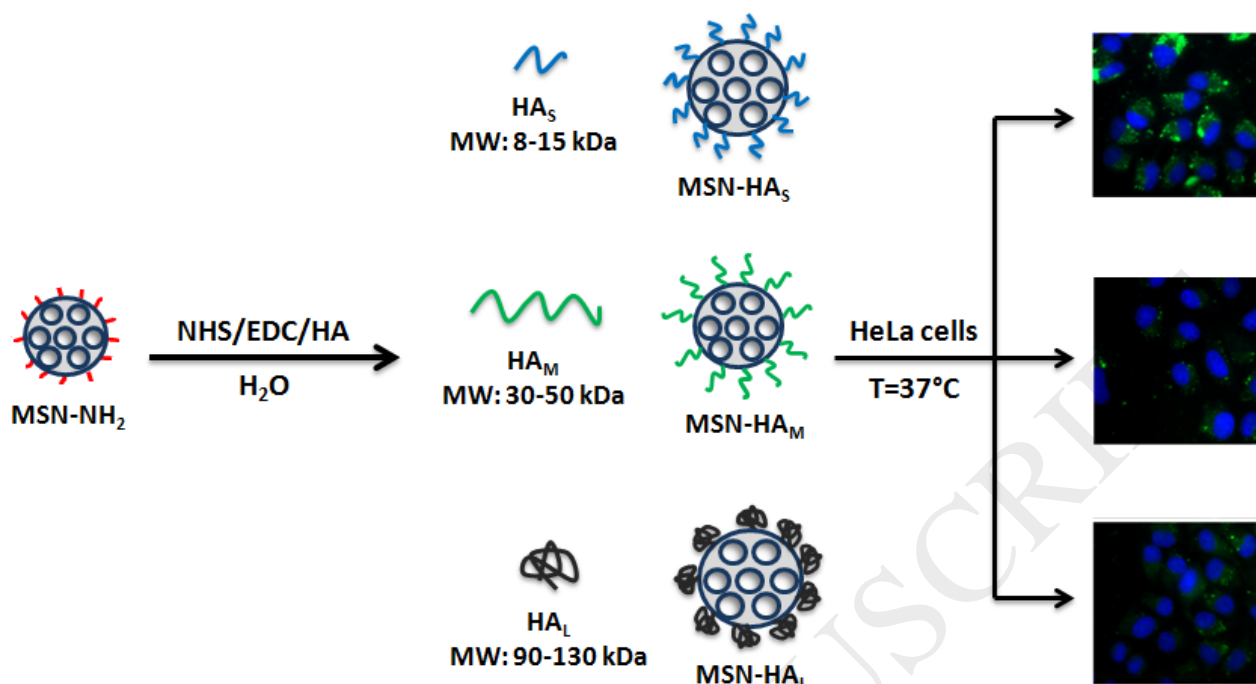
⁴Departamento de Química Inorgánica y Bioinorgánica, Facultad de Farmacia, Universidad Complutense de Madrid, Plaza Ramon y Cajal s/n, Instituto de Investigación Sanitaria Hospital 12 de Octubre i+12 ; Centro de Investigación Biomedica en Red de Bioingeniería, Biomateriales y Nanomedicina (CIBER-BBN), Madrid, Spain

***CORRESPONDING AUTHORS FOOTNOTE.** Tel.: +39070 675 4362/4385. Fax:
+390706754388
Email: asalis@unica.it, monduzzi@unica.it

Statistical summary

- 4587 words (without considering abstract and references)
- 4 figures
- 1 Table

Graphical Abstract:



Highlights:

- Mesoporous silica nanoparticles (MSNs) were functionalized with hyaluronic acid (HA).
- DLS and ELS were used to characterize the hydrodynamic diameter and zeta potential of MSN-HA samples.
- Cell uptake of MSN-HA on HeLa cells was investigated through optical microscopy and TEM.
- The length of HA chain affects the internalization of MSN-HA on HeLa cells.

ABSTRACT

Mesoporous silica nanoparticles (MSNs) were functionalized with amino groups (MSN-NH_2) and then with hyaluronic acid, a biocompatible biopolymer which can be recognized by CD44 receptors in tumor cells, to obtain a targeting drug delivery system. To this purpose, three hyaluronic acid samples differing for the molecular weight, namely HA_S (8 -15 kDa), HA_M (30-50 kDa) and HA_L (90-130 kDa), were used. The MSN-HA_S , MSN-HA_M , and MSN-HA_L materials were characterized through zeta potential and dynamic light scattering measurements at $\text{pH}=7.4$ and $T=37^\circ\text{C}$ to simulate physiological conditions. While zeta potential showed an increasing negative value with the increase of the HA chain length, an anomalous value of the hydrodynamic diameter was observed for MSN-HA_L , which was smaller than that of MSN-HA_S and MSN-HA_M samples. The

cellular uptake of MSN-HA samples on HeLa cells at 37°C was studied by optical and electron microscopy. HA chain length affected significantly the cellular uptake that occurred at a higher extent for MSN-NH₂ and MSN-HA_S than for MSN-HA_M and MSN-HA_L samples. Cellular uptake experiments carried out at 4°C showed that the internalization process was inhibited for MSN-HA samples but not for MSN-NH₂. This suggests the occurrence of two different mechanisms of internalization. For MSN-NH₂ the uptake is mainly driven by the attractive electrostatic interaction with membrane phospholipids, while MSN-HA internalization involves CD44 receptors overexpressed in HeLa cells.

KEYWORDS: Mesoporous silica nanoparticles, Hyaluronic acid, cellular uptake, target system, optical microscopy, transmission electron microscopy.

1. Introduction.

Cancer is a multifactorial widespread disease that represents a growing threat for human health [1]. The microenvironment of solid tumors is very similar to tissue repair sites of an injured tissue where activated platelets are involved in the release of vasoactive mediators, serum fibrinogen, growth factors, and proteins for the regeneration of a new healthy tissue. In particular epithelial and stromal cells are involved in a reciprocal signaling cross-talk responsible of the healing which is interrupted when the tissue is completely regenerated, while persists in tumor tissue allowing for the growth of tumor and stimulating the angiogenesis [2–4]. This phenomenon takes place in solid tumors when they reach 2 mm^3 , and causes the formation of new blood vessels [5]. Long-circulating nanosized drug delivery systems (NDDS) can take advantage of the abnormal vascularization of tumor tissues. Indeed endothelial pores have dimensions between 10 and 1000 nm, and lymphatic vessels in tumor tissue are absent or no-functional, hence NDDS cannot efficiently be removed and are retained inside the endothelial pores. This passive phenomenon is known as Enhanced Permeability and Retention (EPR) effect [5].

Current therapies consist in the administration of chemotherapeutic drugs that are able to curb tumor growth, but these drugs are toxic for healthy cells and can produce several bad side effects [1,2]. In the recent years researchers widely focused on the possibility to produce site-specific drug nanocarriers. Several smart drug delivery systems based on functionalized liposomes [6,7], micelles [8], mesoporous silica nanoparticles [9–12], carbon nanotubes [13], and inorganic nanoparticles [14] have been engineered. These systems allow to address the drug administration to the diseased tissue only [5,7], thus obtaining a reduction of the toxic effects of the drug along with an increase of the local drug concentration, and consequently an improvement of the therapeutic efficacy [15].

In this context ordered mesoporous silica was used for the first time in 2001 by Vallet-Regi and co-workers [16], and, as a result of peculiar features such as high surface area and pore volume that allow for drug adsorption and controlled release, received great attention since then [10,11,17–25].

Moreover, the possibility to introduce smart functional groups at the internal and/or the external mesoporous silica surface [9,26–28] allows to promote different types of specific interactions with biological entities. Focusing on mesoporous silica nanoparticles (MSNs), huge improvements were obtained on specific actions such as the MSNs' performance towards the sustained drug release [9,26–28], the reduction of toxicity, the increase of the biocompatibility [10,29,30] and cell internalization [31], as well as the cytotoxicity towards tumor cells [32,33]. Indeed, several target molecules [10,17,30,34–37] and stimuli-responsive capping agents [27,34,38–41] can easily be grafted at the MSNs' surface. Target molecules allow the MSNs to reach the tumor tissue only through a molecular recognition mechanism. Then, once in the internal tissue, the stimuli-responsive capping agent [5,34] permits the release of the drug as a response to internal (change of pH [42–45], temperature [46–48], redox reactions [40,49–52]) or external (irradiation with light [53–55], magnetic field [55–57]) stimuli.

Hyaluronic acid (HA) is an anionic polysaccharide composed of D-glucuronic acid and N-acetyl-D-glucosamine units linked through alternating $\beta_{1,3}$ and $\beta_{1,4}$ glycosidic bonds [58,59]. HA is the main component of the extracellular matrix of the human connective tissue and one of the most important components of the skin. It also occurs at high concentrations in synovial joint fluids, vitreous humor of eyes, hyaline cartilage, intervertebral disc nucleus, and umbilical cord [59]. In humans HA is synthesized in plasma membrane by membrane-bound synthase (Has) [58]. This enzyme is present in three different isoforms: Has1 and Has2, responsible for the synthesis of high molecular weight HA ($\sim 2 \cdot 10^6$ Da), and Has3, responsible of low molecular weight ($< 3 \cdot 10^5$ Da) [58,60,61]. HA has also many physiological roles related to its structure as for example regulation of water in tissues, lubrication, structural and space-filling properties. If modifications of HA ordered structure occur, the physicochemical properties, being controlled by HA's secondary and tertiary structure, also change, particularly the rheological behavior [58]. Furthermore HA has a very good affinity for CD44 receptors overexpressed in several cancer cells, property that makes it a great active tumor

target [2,62]. Recently HA was used to target different kinds of NDDS like HA-conjugated polyamidoamine dendrimers [63], micelles [64], and ceramides [65] or HA-grafted graphene quantum dots [66], carbon nanotubes [67,68] as well as mesoporous silica nanoparticles [69].

Herein the behavior of HA-grafted MSNs was investigated, focusing on the effects of the biopolymer's chain length towards cell internalization. MSNs were functionalized with HA having different molecular weight: HA_S: 8-15 kDa, HA_M: 30-50 kDa and HA_L: 90-130 kDa. Dynamic (DLS) and electrophoretic (ELS) light scattering measurements were used to characterize the different systems at pH=7.4 at the temperature of 37°C to simulate physiological conditions [45,70–72]. Fluorescence and electron microscopy experiments were then performed to highlight the effects of the polymer's chain length on the HA-grafted MSNs' internalization in HeLa cells.

2. Materials and methods

2.1. Chemicals

Tetraethoxysilane (TEOS, 98%), hexadecyltrimethylammonium bromide (CTAB, > 99 %), anhydrous toluene (99.8 %), 3-aminopropyl-triethoxysilane (APTES, > 98 %), hydrochloride acid (37%), fluorescein isothiocyanate (FITC) and triethylamine (> 99 %) were purchased from Sigma-Aldrich (Milan, Italy). NH₄NO₃ (> 99.9 %), NaH₂PO₄ (99 %), Na₂HPO₄ (99 %), acetic acid (>99.7%), NaOH (97 %), *N*-(3-dimethylaminopropyl)-*N'*-ethylcarbodiimide hydrochloride (EDC, > 98 %), *N*-hydroxysuccinimide (NHS, > 97 %) were purchased from Fluka. Hyaluronic acid sodium salt (HA_S: 8-15 kDa, HA_M: 30-50 kDa and HA_L: 90-130 kDa) was purchased from Contipro Biotech a.s. (Czech Republic).

2.2. Synthesis of amino-functionalized Mesoporous Silica Nanoparticles (MSN-NH₂)

A mass of 1 g of CTAB was dissolved in 480 g of Millipore water and 3.5 mL of NaOH (2 M) and the resulting solution was stirred at 80°C. After 2 h a volume of 10 mL of TEOS was added dropwise. The solution was stirred for other 2 h, and then the resulting white precipitate (MSN-T) was filtered under vacuum, washed with distilled water and methanol, and dried overnight at room temperature. The grafting of the amino group on the surface of the MSNs was carried out by dispersing 1 g of the MSN-T sample in 45 mL of anhydrous toluene, and then adding dropwise 0.5 mL of APTES. The dispersion was stirred and kept at 110°C under reflux overnight. The resulting MSN-T-NH₂ sample was collected by filtration, washed with acetone, and dried overnight at room temperature under vacuum. CTAB surfactant was removed by dispersing the previously synthesized material in 1L of a 10 mg/mL NH₄NO₃ solution in ethanol:water (95:5), and then stirring the dispersion overnight under reflux. The functionalized mesoporous silica nanoparticles (MSN-NH₂) were recovered via filtration, washed with water and ethanol, and dried under vacuum at room temperature. The removal of CTAB is confirmed by the disappearance from FTIR spectra (Fig. S1) of the bands at 2930 cm⁻¹ and 2840 cm⁻¹ - assigned to asymmetric and symmetric stretching of C-H, respectively - the band at 1490 cm⁻¹, due to the C-H bending, and that at 1220 cm⁻¹ assigned to the C-N stretching of CTAB molecule.

2.3 Grafting of Hyaluronic Acid (HA) on MSN-NH₂

A mass of 0.5 g of MSN-NH₂ sample was dispersed in 50 mL of millipore water. In another vessel, 10 mL of an aqueous solution containing NHS (0.186 g) and EDC (0.113 g) were mixed with 30 mL of an aqueous solution containing 0.060g of HA at different chain length (HA_S, HA_M and HA_L). The two solutions were mixed, and the pH was adjusted to 9.0 by adding triethylamine. Finally, the mixture was stirred at 38°C overnight. The HA-modified MSNs (MSN-HA_S, MSN-HA_M and MSN-

HA_L) were collected after centrifugation, washed extensively with millipore water, and dried under vacuum and at room temperature overnight.

FITC labeling of functionalized MSNs was carried out by dispersing 40 mg of MSN-NH₂ or HA-grafted MSNs (MSN-HA_S, MSN-HA_M and MSN-HA_L) in 5 mL of a 3.75 mM FITC solution in ethanol. The dispersion was stirred at room temperature under dark conditions for 3h. The obtained yellow powder was centrifuged, washed with ethanol to remove the excess of FITC, and dried under vacuum. These FITC labeled MSNs were used for fluorescence microscopy.

2.4. Physico-chemical characterization of functionalized MSNs

Textural analysis was carried out on an ASAP 2020 instrument, by determining the N₂ adsorption/desorption isotherm at 77 K. Before analysis functionalized MSNs samples were heated at 40°C, at the rate of 1°C/min, under vacuum for 60h. The Brunauer-Emmett-Teller (BET)[73] and Barrett-Joyner-Halenda (BJH)[74] methods, calculated from adsorption and desorption branch of N₂ isotherm, were used to calculate surface area, pore volume and pore size distribution, respectively.

Small-angle X-ray scattering (SAXS) patterns were recorded through a S3-MICRO SWAXS camera system (HECUS X-ray Systems, Graz, Austria). CuK α radiation of wavelength 1.542 Å was provided by a GeniX-X-ray generator, operating at 30 kV and 0.4 mA. A 1D-PSD-50M system (HECUS X-ray Systems, Graz, Austria) containing 1024 channels of width 54.0 µm was used for detection of scattered X-rays in the small-angle region. The working q -range (Å⁻¹) was $0.003 \leq q \leq 0.6$, where $q (=4\pi\sin\theta/\lambda)$ is the modulus of the scattering wave vector and θ is the scattering angle. Thin-walled 2 mm glass capillaries were filled with the sample for the scattering experiments. The scattering patterns were recorded for 1 h.

Thermogravimetric analysis (TGA) was carried out on a TG-DTA 320 Seiko thermo-balance. Thermal analysis data were collected in the 25–1000 °C range, under oxygen flow (heating rate = 10 °C·min⁻¹; flow rate = 50 mL·min⁻¹).

The hydrodynamic diameter (d_H) and the zeta potential (ζ) of MSNs were measured using a Zetasizer Nano ZSP (Malvern Instruments) in backscatter configuration ($\theta = 173^\circ$), at laser wavelength of $\lambda = 633$ nm. The scattering cell temperature was fixed at 37°C, and the data were analyzed with the Zetasizer software 7.03 version. For both d_H and ζ measurements the sample was prepared by suspending MSNs (1 mg/mL) in filtered (0.2 μ m polypropylene filter, Whatman) milliQ water, 25 mM phosphate buffer (pH 7.4). Samples were sonicated for 30 min and left under stirring overnight. The samples were sonicated for other 30 min and then the measurements were carried out. ζ -potential values were calculated by mean of the Henry equation [75]:

$$\mu_E = \frac{2\varepsilon\zeta f(ka)}{3\eta} \quad (1)$$

where μ_E is the electrophoretic mobility, η is the viscosity of the dispersant, and $f(ka)$ the Henry's function, ε ($=\varepsilon_0\varepsilon_r$) is water permittivity and ε_0 ($= 8.85$ pF/m) is vacuum permittivity. For our experiments we assumed as dispersant water ($\varepsilon_r = 78.5$ at 25 °C and 74.40 at 37 °C, and $\eta = 0.89$ cP at 25°C and 0.69 cP at 37 °C) and $f(ka)=1.5$ in agreement with Smoluchowski approximation commonly used for nanoparticles larger than 0.2 μ m dispersed in aqueous media and with electrolytes concentration higher than 10 mM.

Fourier transform infrared (FTIR) studies were carried out with a Bruker Tensor 27 spectrophotometer equipped with a diamond-ATR accessory and a DTGS detector. A number of 256 scans at a resolution of 2 cm⁻¹ were averaged from wave number 4000 to 400 cm⁻¹. The Opus software was used for data handling.

2.5. Biological assays

The human cervical carcinoma HeLa cell line and 3T3 murine fibroblasts (kindly provided by Dr. A. Diana, University of Cagliari) were grown in DMEM medium supplemented with 10% fetal bovine serum (FBS), 2mM L-Glutamine, penicillin (100U/mL) and streptomycin(100µg/mL) at 37°C in 5% CO₂.

Cell Growth was evaluated culturing 3×10^4 /mL Hela cells in 12 well plates. The day after ($t = 0$) cells were treated with 50 µg/mL of MSN-NH₂, and with HA-modified MSNs (MSN-HA_S, MSN-HA_M and MSN-HA_L). After 24 h nanoparticles were removed, and cells were cultured with fresh medium. Cell counts were performed immediately ($t = 24$ h), after 24 ($t = 24$ h + 24 h) and 48 ($t = 24$ h + 48 h) hours following nanoparticles removal, using a Scepter Cell Counter, Millipore. All the experiments were performed at least in triplicate for each group.

For fluorescence microscopy, HeLa cells were grown in Dulbecco's Modified Eagle's Medium (DMEM; Sigma Aldrich) supplemented with fetal calf serum (10%) at 37°C in a humidified atmosphere containing 5 % CO₂. Cells were seeded in 3 cm dishes containing glass coverslips at a density of 1×10^5 /mL, left to grow for 24 h, and then incubated with 50 µg/mL FITC-MSN-NH₂ or FITC-MSN-HA_x, where $x = L$ (long), M (medium), and S (short) HA chain, for varying times (4 and 24 h) either at 37°C or 4°C. After incubation, the cells were washed with PBS to remove unbound nanoparticles, fixed with paraformaldehyde (4%), stained with the nuclear dye Hoechst 33342 and observed through a fluorescence microscope (Olympus BX41) or processed for immunocytochemistry.

For immunocytochemistry assay, cells on coverslips were pre-incubated with normal goat serum (1:5, Vector, Burlingame, CA, USA) for 30 min. Cells were then overlaid for 60 min at room temperature with the mouse anti-CD44 antibody (1:200, Chemicon). Then the cells were washed three times with PBS and subsequently incubated for 1h with an anti-mouse IgG conjugated with Alexa Fluor 594 (1:500, Molecular Probes). Nuclei were counterstained with Hoechst 33342. Negative controls were routinely performed for each experiment, incubating the samples with non-

immune serum and then with appropriate secondary antibody. Imaging was carried out using an Olympus BX41 fluorescence microscope.

A quantitative determination of the cellular uptake was provided by flow cytometry measurement. HeLa cells ($1 \times 10^5/\text{mL}$) seeded in 6 cm plates were grown for 24 h and then treated with FITC-MSN-NH₂ or FITC-MSN-HA (HA_S, HA_M, HA_L) for 4 h either at 37°C or 4°C. After incubation, the cells were washed with PBS, harvested by trypsinization, suspended in PBS and analyzed by a flow cytometer FACSCANTO flow cytometer (BD-Bioscience) and analyzed with FACSDiva software Version 6.1.3 (BD Biosciences) and FloJo V7.6.5 software.

MSNs internalization was also visualized through Transmission Electron Microscopy. Samples of HeLa cells, incubated with MSN-NH₂, and with HA-modified MSNs (MSN-HA_S, MSN-HA_M and MSN-HA_L) for 24 h at 37°, were fixed for 2 hours in a solution of 1% (para)formaldehyde (Electron Microscopy Sciences) and 1.25% glutaraldehyde (Electron Microscopy Sciences) in 0.1 M sodium cacodylate (Electron Microscopy Sciences) buffer, at pH 7.4. After rinsing in the same buffer after fixation, samples were postfixed in 1% osmium tetroxide for 1 h and stained in aqueous uranyl acetate 0.25% overnight at 4°C. Dehydration of cell cultures in a ascending graded series of ethanol and xylene was followed by infiltration and embedding in Epon 812 resin. The specimens were transferred to flat embedding molds and polymerized in an oven at 60 °C for 24 h. Finally, thin sections (60-90 nm thick) were cut with a LKB ultratome 8800 ultramicrotome, post-stained with uranyl acetate and bismuth subnitrate, observed and photographed in a transmission electron microscope (JEOL 100S model, Tokyo, Japan) operating at 80 kV.

3. Results and discussion

Functionalized MSNs, prepared according to methods described in the previous section, were firstly characterized for their structural, textural and surface properties through TEM, SAXS, N₂ adsorption isotherms, along with FTIR, TGA, DLS and ELS experiments. Then, to evaluate

biocompatibility and cell internalization performance, biological assays on HeLa cells were performed using image techniques, namely optical and electron microscopy.

3.1. Characterization of functionalized MSN samples

A TEM micrograph of MSNs is shown in Fig. 1A. The particles are almost spherical and display, as expected, parallel pore channels. The SAXS patterns of MSN-NH₂, MSN-HA_S, MSN-HA_M and MSN-HA_L, shown in Fig. 1B, are typical of hexagonal structures, displaying an intense peak due to reflection of (100) plane and two weak peaks due to the reflection of (110) and (200) planes, respectively. This result confirms that the functionalization preserves the original ordered structure of the materials. The lattice parameters, calculated using the usual equation $a_{\text{Hex}} = (2/3^{0.5}) \times (h^2 + k^2 + l^2)^{0.5}$, are reported in Table 1. The N₂ adsorption/desorption isotherms of MSNs materials are reported in Fig. 1C. They exhibit the typical trend of type IV isotherms, with a sharp increase of gas volume adsorption at relative pressure values in the range 0.2 - 0.4 p/p°. Table 1 reports also the data of surface area (S_{BET}), pore diameter (d_{BJH}) and pore volume (V_{pBJH}), whereas Fig. S2A shows the pore size distribution obtained for the functionalized materials. The FTIR spectra reported in Fig. 1D for the same samples show the characteristic peaks of silica materials, two peaks at 1060 cm⁻¹ and 800 cm⁻¹ due to the asymmetric and symmetric stretching vibration of Si-O-Si, respectively, and other two at 450 cm⁻¹ and 960 cm⁻¹ that can be related to O-Si-O bending and Si-OH stretching, respectively [76,77]. Surface functionalization is confirmed by the presence of two peaks at 1530 and 1640 cm⁻¹ that are related to -NH₂ bending [78] and C=O stretching [79] for NH₂- and HA-modified MSNs, respectively. Concerning the peak at 1640 cm⁻¹, it cannot be excluded that it could also be due to the C=O stretching of NHS used to activate the -COOH groups of HA. Nonetheless, NHS is soluble in water and its excess has likely been fully removed during the last synthesis step where an extensive washing of the sample was carried out. In any case the functionalization of MSN-NH₂ with HA is confirmed by TGA and ELS measurements as described

below. Fig. S2B displays the percentage mass loss as a function of temperature for functionalized MSNs. Values of mass loss below and above 200°C are reported in Table 1. For temperature below 200°C mass loss is due to the removal of humidity and to the condensation of surface silanols. More interesting are the results at temperature above 200°C when organic groups are burnt, although the mass loss measured for MSN-HA_L is relatively low compared to those found particularly for MSN-HA_M sample.

Figure 1

3.2. Electrophoretic (ELS) and dynamic (DLS) and light scattering measurements

The functionalized MSNs materials were also characterized through electrophoretic light scattering (ELS) (Fig. S2C) and dynamic light scattering DLS (Fig. S2D) measurements to highlight the effects of the external functionalization. As reported in Table 1 and in Fig. S2C, ζ values change as a result of the functionalization with the biopolymer. Indeed the positive value obtained for MSN-NH₂ (+34 mV) becomes negative for MSN-HA systems, due to the presence of carboxylic groups in the biopolymer's chain. Furthermore ζ values become more negative with increasing the length of HA's chain, and then the number of dissociated carboxylic groups as demonstrated by the basic pH values. From DLS measurements we would expect an increase, of the particle's size, d_H (Table 1, and Fig. S2D) along the series: MSN-NH₂ < MSN-HA_S < MSN-HA_M < MSN-HA_L. In fact, d_H increased going from MSN-NH₂ (160±6 nm) to MSN-HA_S (192±15 nm), but remained unchanged for MSN-HA_M (197±8 nm), and decreased for MSN-HA_L (168±11 nm) as obtained through DLS analysis. The increase of biopolymer chain length, going from HA_S (MW = 8-15 kDa) to HA_M (MW = 30-50 kDa), and to HA_L (MW = 90-130 kDa) increases the probability of a multi-point attachment of HA on MSN-NH₂ which simply does not allow the full disentanglement of the biopolymer chain. This is likely the reason of the counterintuitive trend of measured d_H values. However, independently of the hydrodynamic diameter and HA's MW, all grafted-HA MSNs produce the inversion of the zeta potential. This was ζ = +34 mV for MSN-NH₂ and became negative for MSN-HA samples (ζ = - 11, -17, -20 mV for short, medium, and long HA) paralleled by a strong increase of pH (from 4.2 to 8.5-8.7), as a result of a high number of dissociated carboxylic groups. The long biopolymer chains of HA_L, multi-point attached and entangled over the MSN-NH₂ surface may produce a thick layer that increases the negative ζ , but does not enlarge the average particle's diameter of MSN-HA_L sample significantly.

In the perspective of using MSNs in biological media, the observation that HA grafting on the MSN-NH₂ surface produces a strong effect on the pH of the aqueous dispersions of the

functionalized MSNs, suggested to deepen the characterizations evaluating the effect of pH using a pH buffer, at 37°C. The functionalized MSNs suspended in water, 25 mM phosphate buffer at pH=7.4 (PhB) were examined at 37°C through ELS and DLS. The results are presented in Fig. 2 and Table S1.

Figure 2

As expected in water medium at 37 °C, ζ values are positive for MSN-NH₂ and negative for MSN-HA systems, being the values very similar to those determined at 25 °C. In phosphate buffer at pH 7.4 all functionalized MSNs display negative values of ζ , being the ζ values increasingly negative according to the following sequence: -NH₂ < -HA_S < -HA_M < -HA_L. Comparing these values to those measured in water a significant adsorption of the H₂PO₄⁻ and HPO₄²⁻ anions at the solid surface can be suggested not only for MSN-NH₂ (that is expected as a result of strong electrostatic interactions induced particularly by divalent HPO₄²⁻ anions), but also for HA-grafted MSNs (see ζ values in Table S1): in the latter case the adsorption of buffer anions is likely due to specific interactions originated by van der Waals (non-electrostatic) forces [80–82]. Turning the attention to the particles' size d_H determined through DLS (see Fig. 2B) we may remark the rather high standard deviations of the obtained values (Table S2). Again we observe the apparently anomalous d_H values measured for MSN-HA_L in both media (water, PhB at pH=7.4), as in the case of data at 25°C, reported in Table S1.

3.3 Optical microscopy

To evaluate the cellular uptake, HeLa cells were treated with FITC-conjugated MSN-HA particles and studied by fluorescence microscopy and cytofluorimetry. As shown in Fig. 3, after 4h of treatment at 37°C, all MSN particles were internalized by cells. In particular, MSN-HA uptake is

likely mediated by CD44 receptors, that are highly expressed in HeLa cells, as shown in Fig. 3. In fact, when a similar experiment was performed at 4°C, nanoparticles were not internalized, suggesting that an ATP-dependent endocytosis is involved in MSN-HA uptake which is relatively inactive at low temperatures (Fig. 3) [83]. On the other hand, when HeLa cells were incubated with MSN-NH₂ at 4°C, a strong fluorescence was observed on the surface of cells, likely due to an attractive interaction between positively charged nanoparticles and negatively charged phospholipids of cell membrane (Fig. 3)[84].

Figure 3

Moreover, we compared the cell internalization of MSN-HA in HeLa cells and in a CD44 receptor-negative cell line (3T3 cells). In contrast to HeLa, the rate of MSNs internalization was very low in 3T3 cells after 4 hours incubation with MSN- HAs (Fig. S3), as already observed by Zhao et al. [83] and Wang et al. [85]. This highlights the importance of CD44 receptors to mediate cell uptake. On the other hand, our previous results showed MSN-HA uptake by 3T3 after 24h incubation [29], suggesting that alternative internalization mechanisms may take place in these cells following prolonged MSN-HA exposure.

A quantitative evaluation of the cellular uptake was provided by cytofluorimeter analysis that confirmed results obtained by microscopy (Fig. S4). In addition, cytofluorimetry showed a different rate of internalization, since MSN-NH₂ and MSN-HAs particles were internalized by all cells, whereas both MSN-HA_M and MSN-HA_L were detected only in about 50% of cells. These differences were detected also by fluorescence microscopy after 24h treatment (Fig. S5). MSN particle internalization does not affect cell growth and proliferation as indicated by cell count results (Fig. S6).

3.4 Electron microscopy

TEM experiments highlighted a well preserved ultrastructure of HeLa cells after treatment with MSN particles, being mainly characterized by the presence of a well-developed Golgi apparatus, endoplasmic reticulum and several mitochondria in their cytoplasm. TEM observations confirmed the fluorescence microscopy results, highlighting the presence of functionalized MSNs in the cytoplasm of the HeLa cells after treatment with all types of particles (Fig. 4) [31,86]. No MSNs were detected in the nuclear compartment (Fig. 4).

Figure 4

The MSNs were found confined within cytoplasmic vesicles delimited by a single membrane, suggesting an endocytosis process for all types of functionalized particles. This mechanism of internalization was proposed also by Guo and co-workers [87] which explained how particle size can affect the mechanism and the rate of cellular internalization. Indeed, MSNs with dimensions around 200 nm are easily internalized with an endocytosis process. However, differences concerning the amount of internalized MSNs were observed. In detail, the HeLa cells following the MSN-NH₂ and MSN-HA_S treatment exhibited the larger amount of internalized MSNs and cell surface interacting MSNs (Fig. 4 A-D), whereas only few internalized MSNs were observed following MSN-HA_M, and MSN-HA_L exposure (Fig. 4 E-H). Interestingly, a higher association of MSN-NH₂ to the cellular surface was observed (Fig. 4 B).

The Optical microscopy and TEM results indicate that two different internalization mechanisms occur for MSN-NH₂ and MSN-HA samples. Indeed, while for MSN-NH₂ the uptake is mediated by the electrostatic attraction between the positive surface charge of the material and the negatively charged cell membrane, for MSN-HA samples the uptake is likely mediated by CD44 receptors overexpressed in HeLa cells (Fig. 3). Indeed, the MSN-HA internalization process occurred at 37°C

only, whereas is inhibited at 4°C, likely due to the inactivation of the ATP-dependent endocytosis at low temperature (see Fig.s 3-4).

4. Conclusions

In this work the behavior of different MSNs samples, functionalized with amino groups and HA with increasing chain length ($HA_S > HA_M > HA_L$), was investigated. They showed different ζ and hydrodynamic diameter in distilled water and at pH 7.4. We found an apparently anomalous d_H value of MSN- HA_L , which was smaller than values obtained for the other samples (MSN- HA_S and MSN- HA_M). These smaller d_H values observed for MSN- HA_L are likely due to the high MW and possible multi-point attachment of HA chains entangled over the solid surface [88]. The internalization of MSNs samples on HeLa cells was then evaluated. Cells were incubated at 37°C and 4°C with the MSNs and visualized through optical and electron microscopy. The image findings suggest important details on the internalization mechanism driven by the ATP-dependent endocytosis, and also by CD44 receptors in the case of HA functionalized MSNs. Remarkably, MSN- NH_2 adsorbs at HeLa surface (Fig. 3A) also at low temperature because of a favorable electrostatic interaction. Finally, the chain length has also an effect on internalization efficiency since this was high for MSN- HA_S and low for MSN- HA_L . This is a relevant finding which is important for the realization of targeting drug delivery systems for cancer treatment.

Acknowledgments. Financial supports from, FIR 2016-17, RAS and Fondazione di Sardegna (CUP F72F16003070002, 2017) and MIUR (FFABR 2017) are gratefully acknowledged. V. Nairi thanks MIUR for financing her PhD scholarship. M. Vallet-Regi thanks The European Research Council (Advanced Grant VERDI; ERC-2015-AdG Proposal no. 694160) and Visiting Scientists 2016 program financed by the Regione Autonoma della Sardegna.

References

- [1] J. Zhang, Y. Sun, B. Tian, K. Li, L. Wang, Y. Liang, J. Han, Multifunctional mesoporous silica nanoparticles modified with tumor-shedable hyaluronic acid as carriers for doxorubicin., *Colloids and Surfaces. B, Biointerfaces.* 144 (2016) 293–302. doi:10.1016/j.colsurfb.2016.04.015.
- [2] S. Misra, P. Heldin, V.C. Hascall, N.K. Karamanos, S.S. Skandalis, R.R. Markwald, S. Ghatak, Hyaluronan-CD44 interactions as potential targets for cancer therapy, *FEBS Journal.* 278 (2011) 1429–1443. doi:10.1111/j.1742-4658.2011.08071.x.
- [3] A. Giordano, U. Galderisi, From the Laboratory Bench to the Patient ' s Bedside : An Update on Clinical Trials With Mesenchymal Stem Cells, (2006) 27–35. doi:10.1002/JCP.
- [4] V. Sordi, M.L. Malosio, F. Marchesi, A. Mercalli, R. Melzi, T. Giordano, N. Belmonte, G. Ferrari, B.E. Leone, F. Bertuzzi, G. Zerbini, P. Allavena, E. Bonifacio, L. Piemonti, Bone marrow mesenchymal stem cells express a restricted set of functionally active chemokine receptors capable of promoting migration to pancreatic islets, 106 (2017) 419–428. doi:10.1182/blood-2004-09-3507.Supported.
- [5] F. Danhier, O. Feron, V. Préat, To exploit the tumor microenvironment: Passive and active tumor targeting of nanocarriers for anti-cancer drug delivery, *Journal of Controlled Release.* 148 (2010) 135–146. doi:10.1016/j.jconrel.2010.08.027.
- [6] D. Mehn, P. Iavicoli, N. Cabaleiro, S. Even, F. Caputo, O. Geiss, L. Calzolari, F. Rossi, D. Gilliland, Analytical ultracentrifugation for analysis of doxorubicin loaded liposomes, *International Journal of Pharmaceutics.* 523 (2017) 320–326. doi:10.1016/j.ijpharm.2017.03.046.

- [7] S. Matviykov, M. Buscema, T. Mészáros, G. Gerganova, T. Pfohl, A. Zumbühl, J. Szebeni, B. Müller, Liposomes: Bio-inspired nano-containers for physically triggered targeted drug delivery, *Proceedings of SPIE - The International Society for Optical Engineering*. 10162 (2017) 1–14. doi:10.1117/12.2258378.
- [8] P. Kumari, O.S. Muddineti, S.V.K. Rempicharla, P. Ghanta, A.K. B B N, B. Ghosh, S. Biswas, Cholesterol-conjugated poly(D, L-lactide)-based micelles as a nanocarrier system for effective delivery of curcumin in cancer therapy, *Drug Delivery*. 24 (2017) 209–223. doi:10.1080/10717544.2016.1245365.
- [9] V. Nairi, L. Medda, M. Monduzzi, A. Salis, Adsorption and release of ampicillin antibiotic from ordered mesoporous silica, *Journal of Colloid and Interface Science*. 497 (2017) 217–225. doi:10.1016/j.jcis.2017.03.021.
- [10] G. Villaverde, A. Baeza, G.J. Melen, A. Alfranca, M. Ramirez, M. Vallet-Regí, A new targeting agent for the selective drug delivery of nanocarriers for treating neuroblastoma, *J. Mater. Chem. B*. 3 (2015) 4831–4842. doi:10.1039/C5TB00287G.
- [11] L.B. de O. Freitas, L. de M. Corgosinho, J.A.Q.A. Faria, V.M. dos Santos, J.M. Resende, A.S. Leal, D.A. Gomes, E.M.B. de Sousa, Multifunctional mesoporous silica nanoparticles for cancer-targeted, controlled drug delivery and imaging, *Microporous and Mesoporous Materials*. 242 (2017) 271–283. doi:10.1016/j.micromeso.2017.01.036.
- [12] V. Nairi, S. Medda, M. Piludu, M.F. Casula, M. Vallet-Regí, M. Monduzzi, A. Salis, Interactions between bovine serum albumin and mesoporous silica nanoparticles functionalized with biopolymers, *Chemical Engineering Journal*. (2018). doi:10.1016/j.cej.2018.01.011.
- [13] R. ling Qi, X. jiao Tian, R. Guo, Y. Luo, M. wu Shen, J. yong Yu, X. yang Shi, Controlled

release of doxorubicin from electrospun MWCNTs/PLGA hybrid nanofibers, *Chinese Journal of Polymer Science (English Edition)*. 34 (2016) 1047–1059. doi:10.1007/s10118-016-1827-z.

- [14] A. Di Martino, O.A. Guselnikova, M.E. Trusova, P.S. Postnikov, V. Sedlarik, Organic-inorganic hybrid nanoparticles controlled delivery system for anticancer drugs, *International Journal of Pharmaceutics*. 526 (2017) 380–390. doi:10.1016/j.ijpharm.2017.04.061.
- [15] H. Chen, D. Liu, Z. Guo, Endogenous Stimuli-responsive Nanocarriers for Drug Delivery, *Chemistry Letters*. 45 (2016) 242–249. doi:10.1246/cl.151176.
- [16] M. Vallet-Regí, A. Rámila, R.P. Del Real, J. Pérez-Pariente, A new property of MCM-41: Drug delivery system, *Chemistry of Materials*. 13 (2001) 308–311. doi:10.1021/cm0011559.
- [17] L. Palanikumar, E.S. Choi, J.Y. Cheon, S.H. Joo, J.-H. Ryu, Noncovalent Polymer-Gatekeeper in Mesoporous Silica Nanoparticles as a Targeted Drug Delivery Platform, *Advanced Functional Materials*. 25 (2015) 957–965. doi:10.1002/adfm.201402755.
- [18] L. Chen, Z. Zhang, X. Yao, X. Chen, X. Chen, Intracellular pH-operated mechanized mesoporous silica nanoparticles as potential drug carriers, *Microporous and Mesoporous Materials*. 201 (2015) 169–175. doi:10.1016/j.micromeso.2014.09.023.
- [19] J.L. Paris, M.V. Cabanas, M. Manzano, M. Vallet-Regí, Polymer-Grafted Mesoporous Silica Nanoparticles as Ultrasound-Responsive Drug Carriers, *ACS Nano*. 9 (2015) 11023–11033. doi:10.1021/acsnano.5b04378.
- [20] A. Maleki, H. Kettiger, A. Schoubben, J.M. Rosenholm, V. Ambroggi, M. Hamidi, Mesoporous silica materials: From physico-chemical properties to enhanced dissolution of poorly water-soluble drugs, *Journal of Controlled Release*. 262 (2017) 329–347.

doi:10.1016/j.jconrel.2017.07.047.

- [21] M. Piras, A. Salis, M. Piludu, D. Steri, M. Monduzzi, 3D vision of human lysozyme adsorbed onto a SBA-15 nanostructured matrix, *Chemical Communications*. 47 (2011) 7338. doi:10.1039/c1cc11840d.
- [22] M. Piludu, L. Medda, F. Cugia, M. Monduzzi, A. Salis, Silver Enhancement for Transmission Electron Microscopy Imaging of Antibody Fragment–Gold Nanoparticles Conjugates Immobilized on Ordered Mesoporous Silica, *Langmuir*. 31 (2015) 9458–9463. doi:10.1021/acs.langmuir.5b02830.
- [23] M. Monduzzi, S. Lampis, S. Murgia, A. Salis, From self-assembly fundamental knowledge to nanomedicine developments, *Advances in Colloid and Interface Science*. 205 (2014) 48–67. doi:10.1016/j.cis.2013.10.009.
- [24] M.S. Bhattacharyya, P. Hiwale, M. Piras, L. Medda, D. Steri, M. Piludu, A. Salis, M. Monduzzi, Lysozyme Adsorption and Release from Ordered Mesoporous Materials, *The Journal of Physical Chemistry C*. 114 (2010) 19928–19934. doi:10.1021/jp1078218.
- [25] D. Steri, M. Monduzzi, A. Salis, Ionic strength affects lysozyme adsorption and release from SBA-15 mesoporous silica, *Microporous and Mesoporous Materials*. 170 (2013) 164–172. doi:10.1016/j.micromeso.2012.12.002.
- [26] Y. Yan, J. Fu, X. Liu, T. Wang, X. Lu, Acid-responsive intracellular doxorubicin release from click chemistry functionalized mesoporous silica nanoparticles, *RSC Adv*. 5 (2015) 30640–30646. doi:10.1039/C5RA00059A.
- [27] Y. Wang, Q. Zhao, N. Han, L. Bai, J. Li, J. Liu, E. Che, L. Hu, Q. Zhang, T. Jiang, S. Wang, Mesoporous silica nanoparticles in drug delivery and biomedical applications,

- Nanomedicine: Nanotechnology, Biology and Medicine. 11 (2015) 313–327.
doi:10.1016/j.nano.2014.09.014.
- [28] P. Yang, S. Gai, J. Lin, Functionalized mesoporous silica materials for controlled drug delivery., *Chemical Society Reviews*. 41 (2012) 3679–98. doi:10.1039/c2cs15308d.
- [29] G. Zhou, L. Li, J. Xing, J. Cai, J. Chen, P. Liu, N. Gu, M. Ji, Layer-by-layer construction of lipid bilayer on mesoporous silica nanoparticle to improve its water suspensibility and hemocompatibility, *Journal of Sol-Gel Science and Technology*. 82 (2017) 490–499. doi:10.1007/s10971-017-4330-2.
- [30] F. Danhier, O. Feron, V. Préat, To exploit the tumor microenvironment : Passive and active tumor targeting of nanocarriers for anti-cancer drug delivery, *Journal of Controlled Release*. 148 (2015) 135–146. doi:10.1016/j.jconrel.2010.08.027.
- [31] A. Salis, M. Fanti, L. Medda, V. Nairi, F. Cugia, M. Piludu, V. Sogos, M. Monduzzi, Mesoporous Silica Nanoparticles Functionalized with Hyaluronic Acid and Chitosan Biopolymers. Effect of Functionalization on Cell Internalization, *ACS Biomaterials Science & Engineering*. 2 (2016) 741–751. doi:10.1021/acsbiomaterials.5b00502.
- [32] S. Williams, A. Neumann, I. Bremer, Y. Su, G. Dräger, C. Kasper, P. Behrens, Nanoporous silica nanoparticles as biomaterials: evaluation of different strategies for the functionalization with polysialic acid by step-by-step cytocompatibility testing, *Journal of Materials Science: Materials in Medicine*. 26 (2015). doi:10.1007/s10856-015-5409-3.
- [33] Y. Yan, J. Fu, T. Wang, X. Lu, Controlled release of silyl ether camptothecin from thiol-ene click chemistry-functionalized mesoporous silica nanoparticles, *Acta Biomaterialia*. 51 (2017) 471–478. doi:10.1016/j.actbio.2017.01.062.

- [34] A. Baeza, M. Colilla, M. Vallet-Regí, Advances in mesoporous silica nanoparticles for targeted stimuli-responsive drug delivery, *Expert Opinion on Drug Delivery*. 12 (2015) 319–337. doi:10.1517/17425247.2014.953051.
- [35] C. de la Torre, I. Casanova, G. Acosta, C. Coll, M.J. Moreno, F. Albericio, E. Aznar, R. Mangues, M. Royo, F. Sancenón, R. Martínez-Máñez, Gated Mesoporous Silica Nanoparticles Using a Double-Role Circular Peptide for the Controlled and Target-Preferential Release of Doxorubicin in CXCR4-Expressing Lymphoma Cells, *Advanced Functional Materials*. 25 (2015) 687–695. doi:10.1002/adfm.201403822.
- [36] Y.-J. Cheng, G.-F. Luo, J.-Y. Zhu, X.-D. Xu, X. Zeng, D.-B. Cheng, Y.-M. Li, Y. Wu, X.-Z. Zhang, R.-X. Zhuo, F. He, Enzyme-Induced and Tumor-Targeted Drug Delivery System Based on Multifunctional Mesoporous Silica Nanoparticles, *ACS Applied Materials & Interfaces*. 7 (2015) 9078–9087. doi:10.1021/acsami.5b00752.
- [37] M. Yu, S. Jambhrunkar, P. Thorn, J. Chen, W. Gu, C. Yu, Hyaluronic acid modified mesoporous silica nanoparticles for targeted drug delivery to CD44-overexpressing cancer cells, *Nanoscale*. 5 (2013) 178–183. doi:10.1039/c2nr32145a.
- [38] A.F. Moreira, D.R. Dias, I.J. Correia, Stimuli-responsive mesoporous silica nanoparticles for cancer therapy: A review, *Microporous and Mesoporous Materials*. 236 (2016) 141–157. doi:10.1016/j.micromeso.2016.08.038.
- [39] N. Zhao, X. Lin, Q. Zhang, Z. Ji, F.J. Xu, Redox-Triggered Gatekeeper-Enveloped Starlike Hollow Silica Nanoparticles for Intelligent Delivery Systems, *Small*. 11 (2015) 6467–6479. doi:10.1002/smll.201502760.
- [40] X. Chen, H. Sun, J. Hu, X. Han, H. Liu, Y. Hu, Transferrin gated mesoporous silica nanoparticles for redox-responsive and targeted drug delivery, *Colloids and Surfaces B*:

Biointerfaces. 152 (2017) 77–84. doi:10.1016/j.colsurfb.2017.01.010.

- [41] L. Tan, H.-X. Wu, M.-Y. Yang, C.-J. Liu, R.-X. Zhuo, The dual-stimulated release of size-selected cargos from cyclodextrin-covered mesoporous silica nanoparticles, *RSC Adv.* 5 (2015) 10393–10399. doi:10.1039/C4RA15574B.
- [42] W.T. Liu, Y. Yang, P.H. Shen, X.J. Gao, S.Q. He, H. Liu, C.S. Zhu, Facile and simple preparation of pH-sensitive chitosan-mesoporous silica nanoparticles for future breast cancer treatment, *Express Polymer Letters.* 9 (2015) 1068–1075. doi:10.3144/expresspolymlett.2015.96.
- [43] D.R. Nogueira, L.E. Scheeren, L.B. Macedo, A.I.P. Marcolino, M. Pilar Vinardell, M. Mitjans, M. Rosa Infante, A.A. Farooqi, C.M.B. Rolim, Inclusion of a pH-responsive amino acid-based amphiphile in methotrexate-loaded chitosan nanoparticles as a delivery strategy in cancer therapy, *Amino Acids.* 48 (2015) 157–168. doi:10.1007/s00726-015-2075-1.
- [44] Z. Li, D.L. Clemens, B.Y. Lee, B.J. Dillon, M.A. Horwitz, J.I. Zink, Mesoporous Silica Nanoparticles with pH-Sensitive Nanovalves for Delivery of Moxifloxacin Provide Improved Treatment of Lethal Pneumonic Tularemia, *ACS Nano.* 9 (2015) 10778–10789. doi:10.1021/acsnano.5b04306.
- [45] A. Popat, J. Liu, G.Q. (Max) Lu, S.Z. Qiao, A pH-responsive drug delivery system based on chitosan coated mesoporous silica nanoparticles, *Journal of Materials Chemistry.* 22 (2012) 11173–11178. doi:10.1039/c2jm30501a.
- [46] X. Kang, Z. Cheng, D. Yang, P. Ma, M. Shang, C. Peng, Y. Dai, J. Lin, Design and synthesis of multifunctional drug carriers based on luminescent rattle-type mesoporous silica microspheres with a thermosensitive hydrogel as a controlled switch, *Advanced Functional Materials.* 22 (2012) 1470–1481. doi:10.1002/adfm.201102746.

- [47] S. Baek, R.K. Singh, T.-H. Kim, J. Seo, U.S. Shin, W. Chrzanowski, H.-W. Kim, Triple Hit with Drug Carriers: pH- and Temperature-Responsive Theranostics for Multimodal Chemo- and Photothermal Therapy and Diagnostic Applications, *ACS Applied Materials & Interfaces*. 8 (2016) 8967–8979. doi:10.1021/acsami.6b00963.
- [48] E. Ugazio, L. Gastaldi, V. Brunella, D. Scalarone, S.A. Jadhav, S. Oliaro-Bosso, D. Zonari, G. Berlier, I. Miletto, S. Sapino, Thermoresponsive mesoporous silica nanoparticles as a carrier for skin delivery of quercetin, *International Journal of Pharmaceutics*. 511 (2016) 446–454. doi:10.1016/j.ijpharm.2016.07.024.
- [49] J.T. Lin, Z.K. Liu, Q.L. Zhu, X.H. Rong, C.L. Liang, J. Wang, D. Ma, J. Sun, G.H. Wang, Redox-responsive nanocarriers for drug and gene co-delivery based on chitosan derivatives modified mesoporous silica nanoparticles, *Colloids and Surfaces B: Biointerfaces*. 155 (2017) 41–50. doi:10.1016/j.colsurfb.2017.04.002.
- [50] Q. Zhao, S. Wang, Y. Yang, X. Li, D. Di, C. Zhang, T. Jiang, S. Wang, Hyaluronic acid and carbon dots-gated hollow mesoporous silica for redox and enzyme-triggered targeted drug delivery and bioimaging, *Materials Science and Engineering: C*. 78 (2017) 475–484. doi:10.1016/j.msec.2017.04.059.
- [51] K. Park, S.S. Park, Y.H. Yun, C.-S. Ha, Mesoporous silica nanoparticles functionalized with a redox-responsive biopolymer, *Journal of Porous Materials*. 24 (2017) 1215–1225. doi:10.1007/s10934-017-0361-x.
- [52] L. Chen, X. Zhou, W. Nie, Q. Zhang, W. Wang, Y. Zhang, C. He, Multifunctional Redox-Responsive Mesoporous Silica Nanoparticles for Efficient Targeting Drug Delivery and Magnetic Resonance Imaging, *ACS Applied Materials & Interfaces*. 8 (2016) 33829–33841. doi:10.1021/acsami.6b11802.

- [53] S. Chai, Y. Guo, Z. Zhang, Z. Chai, Y. Ma, L. Qi, Cyclodextrin-gated mesoporous silica nanoparticles as drug carriers for red light-induced drug release, *Nanotechnology*. 28 (2017) 145101. doi:10.1088/1361-6528/aa5e74.
- [54] G. Wang, J. Dong, T. Yuan, J. Zhang, L. Wang, H. Wang, Visible Light and pH Responsive Polymer-Coated Mesoporous Silica Nanohybrids for Controlled Release, *Macromolecular Bioscience*. 16 (2016) 990–994. doi:10.1002/mabi.201600008.
- [55] W. Li, P. Liao, C. Su, C. Yeh, Formation of Oligonucleotide-Gated Silica Shell-Coated Fe₃O₄-Au Core-Shell Nanotrisoctahedra for Magnetically Targeted and Near-Infrared Light-Responsive Theranostic Platform, *Journal of the American Chemical Society*. 136 (2014) 10062–10075. doi:10.1021/ja504118q.
- [56] W.-H. Chen, G.-F. Luo, Q. Lei, F.-Y. Cao, J.-X. Fan, W.-X. Qiu, H.-Z. Jia, S. Hong, F. Fang, X. Zeng, R.-X. Zhuo, X.-Z. Zhang, Rational design of multifunctional magnetic mesoporous silica nanoparticle for tumor-targeted magnetic resonance imaging and precise therapy, *Biomaterials*. 76 (2016) 87–101. doi:10.1016/j.biomaterials.2015.10.053.
- [57] E. Che, Y. Gao, L. Wan, Y. Zhang, N. Han, J. Bai, J. Li, Z. Sha, S. Wang, Paclitaxel/gelatin coated magnetic mesoporous silica nanoparticles: Preparation and antitumor efficacy in vivo, *Microporous and Mesoporous Materials*. 204 (2015) 226–234. doi:10.1016/j.micromeso.2014.11.013.
- [58] Y.-H. Liao, S.A. Jones, B. Forbes, G.P. Martin, M.B. Brown, Hyaluronan: Pharmaceutical Characterization and Drug Delivery, *Drug Delivery*. 12 (2005) 327–342. doi:10.1080/10717540590952555.
- [59] E.D. Prè, G. Conti, A. Sbarbati, Hyaluronic Acid (HA) Scaffolds and Multipotent Stromal Cells (MSCs) in Regenerative Medicine, *Stem Cell Reviews and Reports*. 12 (2016) 664–

681. doi:10.1007/s12015-016-9684-2.

- [60] N. Itano, K. Kimata, Mammalian Hyaluronan Synthases, IUBMB Life. 1 (2002) 195–199. doi:10.1080/15216540290114478.
- [61] A.P. Spicer, T.K. Nguyen, Mammalian hyaluronan synthases: investigation of functional relationships in vivo, Biochemical Society Transactions. 27 (1999) 109–115. doi:10.1042/bst0270109.
- [62] G. Mattheolabakis, L. Milane, A. Singh, M.M. Amiji, Hyaluronic acid targeting of CD44 for cancer therapy: from receptor biology to nanomedicine, Journal of Drug Targeting. 23 (2015) 605–618. doi:10.3109/1061186X.2015.1052072.
- [63] P. Kesharwani, L. Xie, S. Banerjee, G. Mao, S. Padhye, F.H. Sarkar, A.K. Iyer, Hyaluronic acid-conjugated polyamidoamine dendrimers for targeted delivery of 3,4-difluorobenzylidene curcumin to CD44 overexpressing pancreatic cancer cells, Colloids and Surfaces B: Biointerfaces. 136 (2015) 413–423. doi:10.1016/j.colsurfb.2015.09.043.
- [64] Y. Zhong, K. Goltsche, L. Cheng, F. Xie, F. Meng, C. Deng, Z. Zhong, R. Haag, Hyaluronic acid-shelled acid-activatable paclitaxel prodrug micelles effectively target and treat CD44-overexpressing human breast tumor xenografts in vivo, Biomaterials. 84 (2016) 250–261. doi:10.1016/j.biomaterials.2016.01.049.
- [65] J.-Y. Lee, U. Termsarasab, J.-H. Park, S.Y. Lee, S.-H. Ko, J.-S. Shim, S.-J. Chung, H.-J. Cho, D.-D. Kim, Dual CD44 and folate receptor-targeted nanoparticles for cancer diagnosis and anticancer drug delivery, Journal of Controlled Release. 236 (2016) 38–46. doi:10.1016/j.jconrel.2016.06.021.
- [66] Abdullah-Al-Nahain, J.-E. Lee, I. In, H. Lee, K.D. Lee, J.H. Jeong, S.Y. Park, Target

Delivery and Cell Imaging Using Hyaluronic Acid-Functionalized Graphene Quantum Dots, *Molecular Pharmaceutics*. 10 (2013) 3736–3744. doi:10.1021/mp400219u.

- [67] H. Yao, Y. Zhang, L. Sun, Y. Liu, The effect of hyaluronic acid functionalized carbon nanotubes loaded with salinomycin on gastric cancer stem cells, *Biomaterials*. 35 (2014) 9208–9223. doi:10.1016/j.biomaterials.2014.07.033.
- [68] X. Cao, L. Tao, S. Wen, W. Hou, X. Shi, Hyaluronic acid-modified multiwalled carbon nanotubes for targeted delivery of doxorubicin into cancer cells, *Carbohydrate Research*. 405 (2015) 70–77. doi:10.1016/j.carres.2014.06.030.
- [69] M. Yu, S. Jambhrunkar, P. Thorn, J. Chen, W. Gu, C. Yu, Hyaluronic acid modified mesoporous silica nanoparticles for targeted drug delivery to CD44-overexpressing cancer cells., *Nanoscale*. 5 (2013) 178–83. doi:10.1039/c2nr32145a.
- [70] G. Yan, J. Wang, L. Hu, X. Wang, G. Yang, S. Fu, X. Cheng, P. Zhang, R. Tang, Stepwise targeted drug delivery to liver cancer cells for enhanced therapeutic efficacy by galactose-grafted, ultra-pH-sensitive micelles, *Acta Biomaterialia*. 51 (2017) 363–373. doi:10.1016/j.actbio.2017.01.031.
- [71] C. Luo, J. Sun, B. Sun, Z. He, Prodrug-based nanoparticulate drug delivery strategies for cancer therapy, *Trends in Pharmacological Sciences*. 35 (2014) 556–566. doi:10.1016/j.tips.2014.09.008.
- [72] S. Mura, J. Nicolas, P. Couvreur, Stimuli-responsive nanocarriers for drug delivery, *Nature Materials*. 12 (2013) 991–1003. doi:10.1038/nmat3776.
- [73] S. Brunauer, P.H. Emmett, E. Teller, Adsorption of Gases in Multimolecular Layers, *Journal of the American Chemical Society*. 60 (1938) 309–319. doi:10.1021/ja01269a023.

- [74] E.P. Barrett, L.G. Joyner, P.P. Halenda, The Determination of Pore Volume and Area Distributions in Porous Substances. I. Computations from Nitrogen Isotherms, *Journal of the American Chemical Society*. 73 (1951) 373–380. doi:10.1021/ja01145a126.
- [75] A. Tekrony, D. Cramb, Determination of the mobility of amine- and carboxy-terminated fluospheres and quantum dots by capillary electrophoresis, *Canadian Journal of Chemistry*. 94 (2016) 430–435. doi:10.1139/cjc-2015-0349.
- [76] B.A. Morrow, A.J. McFarlan, Surface vibrational modes of silanol groups on silica, *Journal of Physical Chemistry*. 96 (1992) 1395–1400. doi:10.1021/j100182a068.
- [77] D. Scarano, A. Zecchina, S. Bordiga, F. Geobaldo, G. Spoto, G. Petrini, G. Leofanti, M. Padovan, G. Tozzola, Fourier-Transform Infrared and Raman-Spectra of Pure and Al, B-, Ti- and Fe-Substituted Silicalites: Stretching-Mode Region, *Journal of the Chemical Society-Faraday Transactions*. 89 (1993) 4123–4130. doi:10.1039/ft9938904123.
- [78] F. Sevimli, A. Yılmaz, Surface functionalization of SBA-15 particles for amoxicillin delivery, *Microporous and Mesoporous Materials*. 158 (2012) 281–291. doi:10.1016/j.micromeso.2012.02.037.
- [79] L. Medda, M.F. Casula, M. Monduzzi, A. Salis, Adsorption of Lysozyme on Hyaluronic Acid Functionalized SBA-15 Mesoporous Silica: A Possible Bioadhesive Depot System, *Langmuir*. 30 (2014) 12996–13004. doi:10.1021/la503224n.
- [80] F. Cugia, S. Sedda, F. Pitzalis, D.F. Parsons, M. Monduzzi, A. Salis, Are specific buffer effects the new frontier of Hofmeister phenomena? Insights from lysozyme adsorption on ordered mesoporous silica, *RSC Adv*. 6 (2016) 94617–94621. doi:10.1039/C6RA17356J.
- [81] A. Salis, L. Medda, F. Cugia, M. Monduzzi, Effect of electrolytes on proteins physisorption

- on ordered mesoporous silica materials, *Colloids and Surfaces B: Biointerfaces*. 137 (2016) 77–90. doi:10.1016/j.colsurfb.2015.04.068.
- [82] A. Salis, M. Monduzzi, Not only pH. Specific buffer effects in biological systems, *Current Opinion in Colloid & Interface Science*. 23 (2016) 1–9. doi:10.1016/j.cocis.2016.04.004.
- [83] Q. Zhao, J. Liu, W. Zhu, C. Sun, D. Di, Y. Zhang, P. Wang, Z. Wang, S. Wang, Dual-stimuli responsive hyaluronic acid-conjugated mesoporous silica for targeted delivery to CD44-overexpressing cancer cells, *Acta Biomaterialia*. 23 (2015) 147–156. doi:10.1016/j.actbio.2015.05.010.
- [84] A. Verma, F. Stellacci, Effect of Surface Properties on Nanoparticle-Cell Interactions, *Small*. 6 (2010) 12–21. doi:10.1002/smll.200901158.
- [85] Z. Wang, Y. Tian, H. Zhang, Y. Qin, D. Li, L. Gan, F. Wu, Using hyaluronic acid-functionalized pH stimuli-responsive mesoporous silica nanoparticles for targeted delivery to CD44-overexpressing cancer cells, *International Journal of Nanomedicine*. Volume 11 (2016) 6485–6497. doi:10.2147/IJN.S117184.
- [86] Y. Xia, M. Li, T. Peng, W. Zhang, J. Xiong, Q. Hu, Z. Song, Q. Zheng, In vitro cytotoxicity of fluorescent silica nanoparticles hybridized with aggregation-induced emission luminogens for living cell imaging, *International Journal of Molecular Sciences*. 14 (2013) 1080–1092. doi:10.3390/ijms14011080.
- [87] H. Guo, H. Qian, S. Sun, D. Sun, H. Yin, X. Cai, Z. Liu, J. Wu, T. Jiang, X. Liu, Hollow mesoporous silica nanoparticles for intracellular delivery of fluorescent dye, *Chemistry Central Journal*. 5 (2011) 1–10. doi:10.1186/1752-153X-5-1.
- [88] S. Furlan, G. La Penna, A. Perico, A. Cesàro, Hyaluronan chain conformation and dynamics,

Carbohydrate Research. 340 (2005) 959–970. doi:10.1016/j.carres.2005.01.030.

ACCEPTED MANUSCRIPT

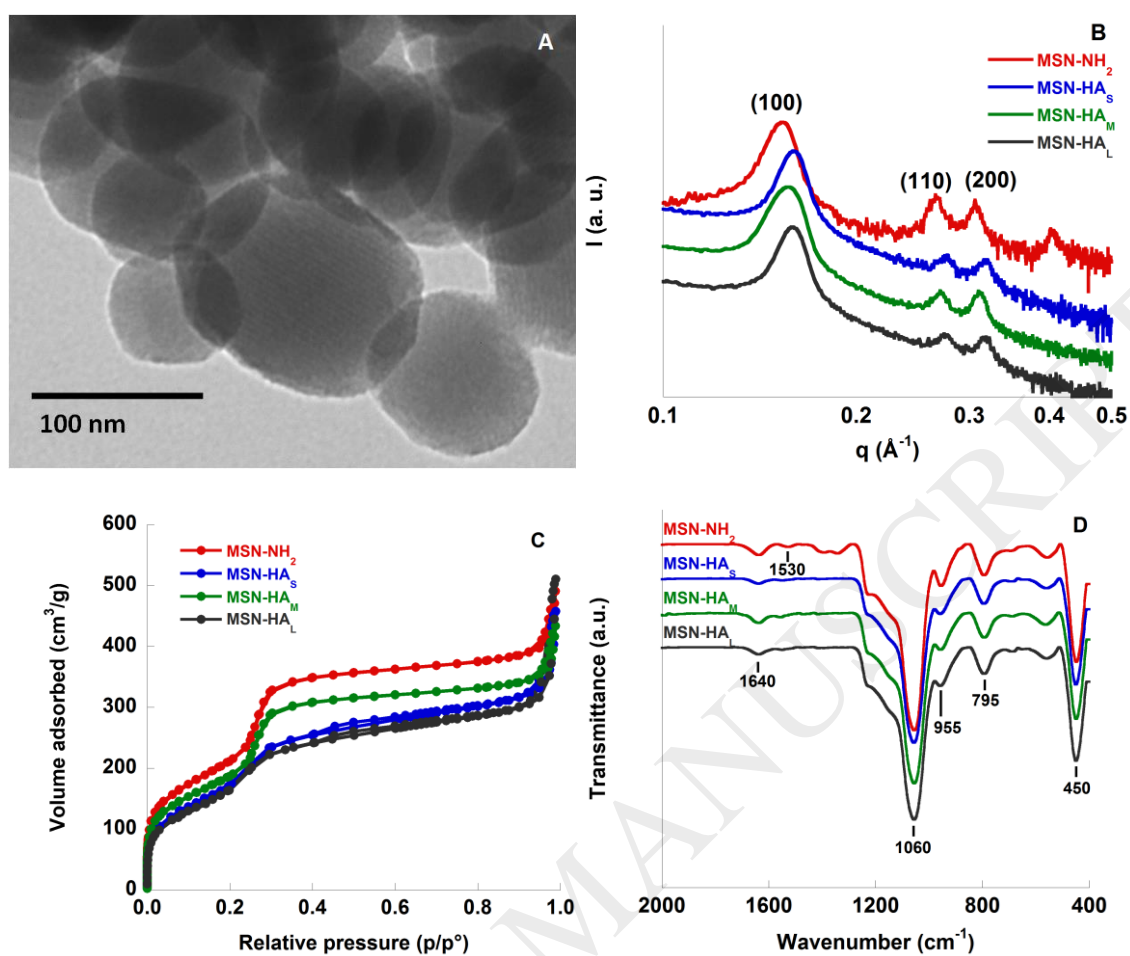
Figures:

Fig. 1 Characterization of Functionalized MSNs: (A) TEM micrographs, (B) SAXS pattern, (C) N₂ Adsorption/desorption isotherms, and (D) FTIR spectra obtained for functionalized MSNs.

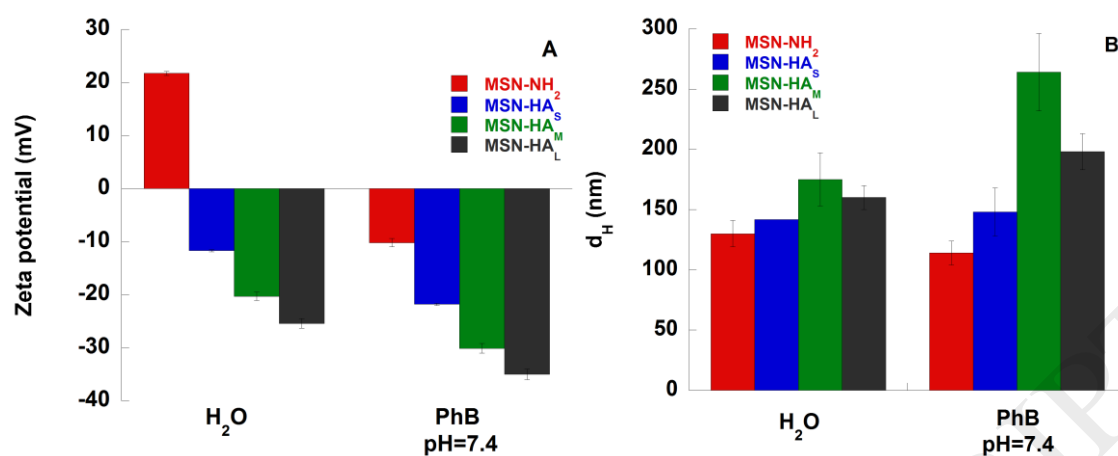


Fig. 2 Functionalized MSNs suspended in water and phosphate buffer PhB at pH 7.4. (A) Zeta potential and (B) hydrodynamic diameter, at 37°C.

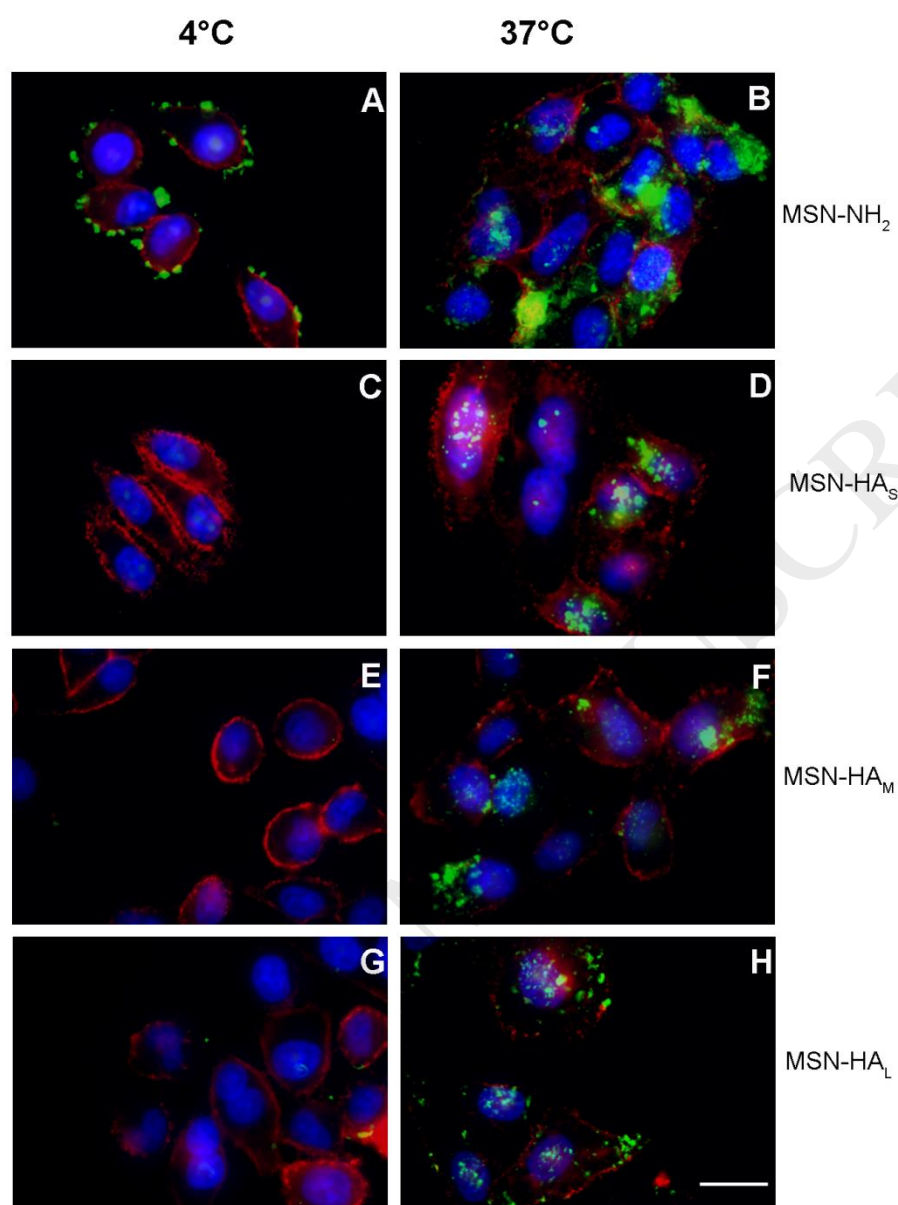


Fig. 3. Fluorescence microscopy images of HeLa cells treated for 4 h at different temperatures (4°C and 37°C) with FITC labeled MSN. Cell membranes are immunostained with CD44 antibody (red) and nuclei are stained with Hoechst (blue). Bar: 20 μ m.

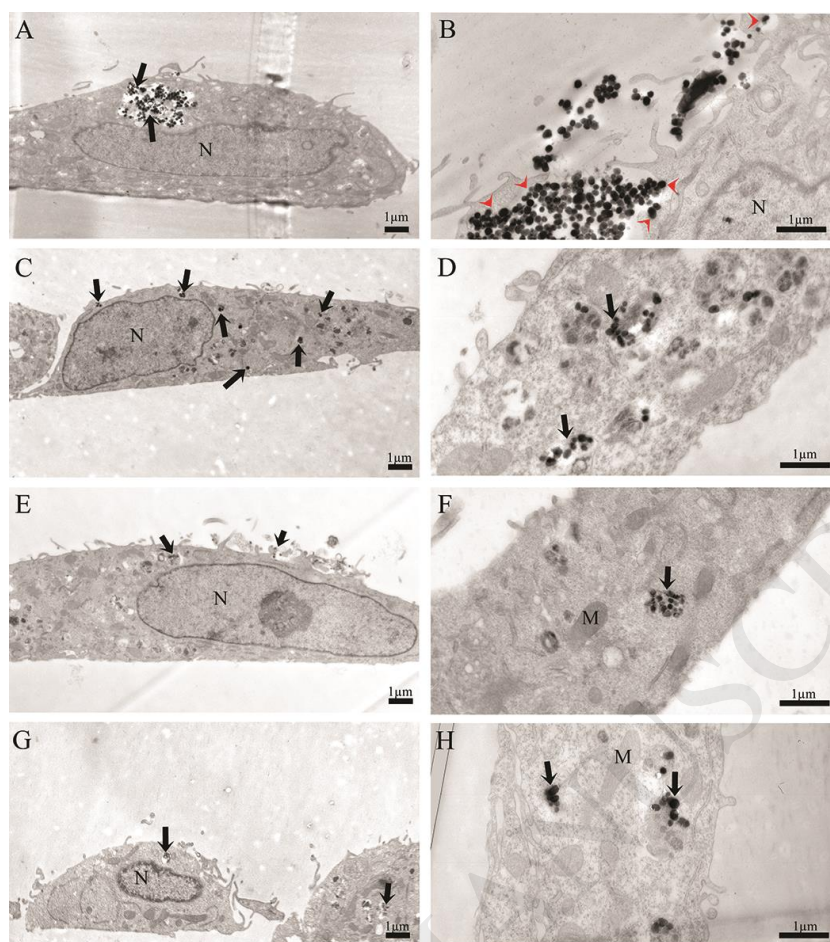


Fig. 4 Electron micrographs of HeLa cells incubated for 24h: (A-B) MSN-NH₂, (C-D) MSN-HA_S, (E-F) MSN-HA_M, (G-H) MSN-HA_L. Black arrows show the presence of the internalized MSNs. (B) Detail of cytoplasmic portion of HeLa cell displaying intense MSN-NH₂ interaction with the external cellular surface (red arrowheads).

Tables:

Table 1. Characterization of functionalized MSNs. Surface area (S_{BET}), pore diameter (d_{BJH}), pore volume (V_{p}), and lattice parameter (a) of Functionalized MSNs. TGA measurements: mass loss (%). pH, zeta potential (ζ) values from ELS, and hydrodynamic diameters (d_{H}) from DLS (in milliQ water at 25°C).

Sample	^a S_{BET} (m^2/g)	^b $d_{\text{Des,BJH}}$ (Å)	^c $V_{\text{pDes,BJH}}$ (cm^3/g)	^d a (Å)	^e Mass loss (%)	^f Mass loss (%)	pH	^e ζ (mV)	^e d_{H} (nm)
MSN- NH ₂	805	23.0	0.64	47.0	10.2	12.0	4.23	+34±1	160±6
MSN- HAs	753	21.3	0.75	45.2	8.0	12.1	8.65	- 11.3±0.2	192±15
MSN- HAm	711	23.0	0.56	43.8	7.6	17.3	8.46	-17±3	197±8
MSN- HAL	735	20.6	0.83	45.4	7.6	15.7	8.73	- 20.4±0.7	168±11

^aSurface area calculated by the BET method. ^bPore diameter from the desorption branch calculated by BJH method. ^cPore volume from the desorption branch calculated at $p/p^\circ=0.99$ by BJH method. ^dLattice parameter obtained by SAXS. ^e $T < 200^\circ\text{C}$. ^f $T > 200^\circ\text{C}$. ^eReported values are the average of at least three measurements.